HHS Public Access

Author manuscript

Nat Commun. Author manuscript; available in PMC 2015 July 08.

Published in final edited form as:

Nat Commun. ; 6: 5974. doi:10.1038/ncomms6974.

Membrane tension and peripheral protein density mediate membrane shape transitions

Zheng Shi[1] and **Tobias Baumgart**[1,*]

[1]Department of Chemistry, University of Pennsylvania, 231 S. 34th St., Philadelphia, PA 19104, USA

Abstract

Endocytosis is a ubiquitous eukaryotic membrane budding, vesiculation, and internalization process fulfilling numerous roles including compensation of membrane area increase after bursts of exocytosis. The mechanism of the coupling between these two processes to enable homeostasis is not well understood. Recently, an ultrafast endocytosis (UFE) pathway was revealed with a speed significantly exceeding classical clathrin-mediated endocytosis (CME). Membrane tension reduction is a potential mechanism by which endocytosis can be rapidly activated at remote sites. Here we provide experimental evidence for a mechanism whereby membrane tension reduction initiates membrane budding and tubulation mediated by endocytic proteins such as endophilin A1. We find that shape instabilities occur at well-defined membrane tensions and surface densities of endophilin. From our data, we obtain a membrane shape stability diagram that shows remarkable consistency with a quantitative model. This model applies to all laterally diffusive curvature coupling proteins and therefore a wide range of endocytic proteins.

Introduction

The cellular processing of signals and cargo is accompanied by the formation of transient, highly curved membrane structures such as tubules and vesicles[1]. One of the best understood membrane transport processes is CME. Among other contributors[2], several types of BAR domain proteins, including endophilin, help induce or stabilize the curvature of clathrin-coated vesicles (CCV)[3]. During clathrin-independent endocytosis, plasma membrane retrieval is modulated by the actions of endophilin and dynamin[4].

Here we correlate the onset of membrane deformation with the number density of BAR-domain proteins on the membrane, and evaluate how membrane tension modifies that relationship. Cellular membrane tensions arise from two primary sources: hydrostatic pressure across the lipid bilayer and cytoskeleton-membrane adhesion[5]. These tensions span a range of values from 0.003 $mN \cdot m^{-1}$ to around 0.3 $mN \cdot m^{-1}$, depending on cell type and

*To whom correspondence should be addressed: T. Baumgart, Department of Chemistry, University of Pennsylvania, 231 South 34th Street, 19104, Philadelphia, PA, USA, Tel.: 215 573 7539; baumgart@sas.upenn.edu.

Author contributions

ZS and TB planned research, ZS conducted experiments, ZS and TB analysed results, ZS and TB wrote manuscript.

state[5–7]. Cells actively maintain their unique membrane tensions and the idea that tension is a regulator of biological processes such as endocytosis has gained attention since the late 1990s[5,8] with significantly more contributions in recent years[6,9–17]. However, in experiments with biological cells, the magnitude of tension has only been coarsely controlled, if it was controlled at all.

Results

We first investigated membrane deformation through the N-terminal BAR domain of endophilin, and then compared these measurements to those obtained with full length endophilin. To enable tension-controlled measurements, a single micropipette-aspirated giant unilamellar vesicle (GUV, labelled with red fluorophores), consisting of a spherical part and an aspirated part (Fig. 1a), was transferred into a solution containing endophilin N-BAR domains (labelled with a green fluorophore) (Fig. 1b)[18]. The protein / membrane binding process was quantified by measuring the increase of green fluorescence signal on the GUV contour, which was converted into the molecular density of proteins on the membrane (see Methods) via a calibration method[19]. Simultaneously, the geometry (aspiration length L_p and vesicle radius R_v, see Fig. 1a) of the GUV was monitored in order to document membrane budding / tubulation transitions induced by N-BAR domain binding. Diameters of membrane tubes induced by N-BAR domains are typically below optical resolution[20], rendering them challenging to image directly, especially during their emergence. However, in our setup, the change in GUV geometry provides a precise indicator for the onset of the membrane shape transition.

Effects of protein density and membrane tension

When a certain amount of endophilin N-BAR domains was bound on the GUV membrane, the aspiration length L_p decreased and membrane tubes grew towards the vesicle exterior until all pipette-aspirated membrane area was consumed (aspiration length $L_p=0$) (Fig. 1c and Supplementary Figure 1). The observed membrane tube formation is consistent with the known capacity of N-BAR proteins to generate membrane curvature[21]. In contrast to the tubulation and corresponding GUV geometry change observed at a membrane tension of 0.05 $mN{\cdot}m^{-1}$ (Fig. 1c), we found that the endophilin N-BAR induced shape instability can be suppressed (Fig.1d) by subjecting vesicles to larger lateral tensions ($\geq$ 0.25 $mN{\cdot}m^{-1}$, see Supplementary theory).

In order to investigate how membrane tension affects tubulation, GUVs covered with endophilin N-BAR were subjected to a range of tensions by varying the pipette aspiration pressures. A vesicle under high tension was first equilibrated in the protein chamber to ensure constant coverage of endophilin N-BAR domain, while suppressing tubulation. The tension of the vesicle was then decreased about threefold within two seconds. When the GUV experienced lower membrane tension, membrane tubes emerged around the vesicle, concomitant with a decrease in L_p (Fig. 1d).

Monitoring vesicle radius and aspiration length allows assessing reductions of visible membrane area as growing tubes consume membrane area from the vesicle geometry. Both the protein-induced and tension change-induced membrane tubulations are correlated with a

decrease in visible GUV membrane area, as calculated from changes in aspiration length and vesicle radius (Fig. 2 and Supplementary Figure 2, also see Methods). However, besides tubulation, the visible membrane area decrease induced by tension reduction has an additional contribution from entropic membrane fluctuations. We show and discuss in Supplementary Figure 3 that effects related to membrane fluctuations are substantially smaller than protein effects.

Determining a shape stability diagram

To obtain an experimental membrane shape stability diagram correlating protein density and membrane tension at the shape transition, GUVs aspirated at a range of membrane tensions were transferred into endophilin N-BAR solutions (Fig. 2). Potential osmotic contributions to changes in vesicle geometry were carefully excluded (Supplementary Figure 2 and Supplementary Figure 4). Consistently, we observed formation of membrane tubes, and the associated decrease in visible membrane area, only after the protein density on GUVs reached a well-defined threshold level, indicating the existence of a protein transition-density required for inducing membrane tubulation. We define the transition-density as the protein density at which visible membrane area of GUVs begins to decrease, as indicated by the arrows in Figure 2. The transition-density has no observable dependence on the protein concentration in the bulk solution (Supplementary Figure 5a). However, comparison between a high tension GUV (Fig. 2a) and a low tension GUV (Fig. 2b) reveals a striking influence of membrane tension on the transition-density with minimal effect on protein-membrane binding (Supplementary Figure 5b). We constructed a membrane shape stability diagram by systematically determining the transition-densities of the protein for GUVs under various membrane tensions (Fig. 3). This stability diagram was obtained for GUVs with the composition DOPS/DOPE/DOPC=45/30/25 with membrane-bound endophilin N-BAR domains. This lipid composition was chosen to mimic the innerleaflet headgroup composition of plasma membranes, where endocytic events take place[22]. Di-oleoyl lipid chains were chosen in order to suppress demixing of lipid mixtures.

We found that full length endophilin shows a qualitatively similar membrane tubulation behaviour as its N-BAR domain, albeit with higher transition-densities compared to the N-BAR domain (Fig. 4), consistent with a potential auto-inhibition of endophilin function[23].

The stability diagram (Fig. 3) illustrates how two factors, density increase (horizontal arrows) and tension decrease (vertical arrows), can be used to control the transformation of lipid membranes from a planar (white) to tubular (dark gray) state. These two trajectories in the stability diagram correspond to the scenarios in Figure 1c and Figure 1d respectively. The stability diagram shows a positive intercept ρ_0 of the stability boundary on the x-axis (displaying number density of N-BAR dimers on the membrane). This is consistent with the fact that at vanishing membrane tension, GUVs with identical lipid compositions in both leaflets are stable towards tubulation in the absence of curvature-inducing proteins.

Analytical model based on three adjustable parameters

We next aim to fit a biophysical model to our data, with the goal to illuminate molecular details of the curvature instability induced by endophilin. We seek the following features of

a suitable model: a) it should allow for locally varying protein densities on the membrane in a temperature-dependent manner, to account for entropic contributions to shape stability; b) it should feature a coupling between local protein density and membrane curvature; c) the exact geometry of the membrane after deformation does not need to be prescribed by the model, because we focus on the onset of the shape instability. While several theories have been developed to explain spontaneous budding/tubulation of membranes[24–26], only the linear stability theory[27] used in the following is consistent with the requirements listed above. Note that the shape of the membrane *after* undergoing the instability would have to be described with a non-linear approach[28].

Using σ to represent the membrane tension, and $\bar{\varphi}$ to represent the average cover fraction of proteins on the membrane (experimentally the cover fraction is obtained by dividing the measured N-BAR dimer density to its close-packed density ρ_{max} = 30000 μm^{-2} [29]), the instability criterion can be written as (see Supplementary theory for details),

$$\sqrt{\sigma} \leq \frac{\kappa C_0}{\sqrt{b}} - \sqrt{\frac{\kappa k_B T}{b\beta}\frac{1}{\bar{\phi}(1-\bar{\phi})^2} + \left(\frac{\kappa^2 {C_0}^2}{b} - \frac{2\kappa\alpha}{b\beta^2}\right)} \quad (1)$$

Here κ is the bending rigidity, C_0 describes the spontaneous curvature of the membrane induced by protein binding (positive for N-BAR domains), k_B is the Boltzmann constant and the T is the temperature. The parameter b is normally a constant and can be expressed in a simple lattice model as $b=\lambda(\beta k_B T)^{-1}$ where β is the excluded area of the protein and λ represents an effective 'interaction area' for molecular interactions in a protein density gradient[30]. The parameter α represents the attraction strength between protein molecules in the two-dimensional Van der Waals model[31].

It follows from Eq. 1 that the experimentally determined stability limit can be fitted with the expression $\sqrt{\sigma}=a_1 - \sqrt{a_2\bar{\phi}^{-1}(1-\bar{\phi})^{-2} + {a_1}^2 - a_3}$, with a_i being parameters that are optimized to yield the best fit with the experimental data. These three fit parameters, a_1 to a_3, are directly related to three molecular properties of the protein: C_0, b, and α (Supplementary equation 11). Furthermore, these molecular properties can be correlated with a set of three measurable physical properties: the protein's membrane curvature coupling strength: κC_0, the maximal tension that allows the curvature instability: σ*, and the protein density required for tubulating a tensionless membrane: ρ_0 (Supplementary equation 12).

As shown in Figure 3, the model is in good agreement with the measured relation between transition-density and membrane tension. In order to be able to obtain the spontaneous curvature from the value of the curvature coupling strength κC_0, we measured the bending rigidity of the membrane used here (DOPS/DOPE/DOPC=45/30/25) as $\kappa = 23\pm3 k_B T$ (Mean ±SD, repeated for five GUVs, also see Methods and Supplementary Figure 6). Assuming β = 50nm^2 [19], the fit results correspond to a spontaneous curvature ${C_0}^{-1}$ = 5.1±0.7nm (here and where not further specified below, uncertainties result from the standard error of fit parameters and error propagation) agreeing well with values inferred from N-BAR protein curvature sorting experiments performed on a GUV-tether system[19,31]. The upper tension

limit for enabling membrane shape transitions through endophilin N-BAR for the lipid composition used here is $\sigma^* = 0.19 \pm 0.04$ mN·m^{-1}. Finally, the protein transition-density required for tubulating a tensionless membrane is $\rho_0 = 650 \pm 150 \mu m^{-2}$, corresponding to about 7.5 protein dimers on a CCV-sized membrane (assuming a CCV radius of 30 nm). Interestingly, the number of endophilin molecules in synaptic boutons was measured in a recent study[32]. An endophilin dimer density of $546 \pm 36 \mu m^{-2}$ on the synaptosome surface can then be estimated (see Supplementary theory for details). This endophilin density turns out to be within the stable regime of the stability diagram (for any membrane tension), but is localized close to the stability boundary (assuming typical neuronal membrane tensions of 0.003 mN·m^{-1} to 0.04 mN·m^{-1} [5]). This suggests that under physiological conditions, the plasma membrane of neuronal cells can easily switch between stable (endocytosis suppressed) and unstable (endocytosis activated) states by changing membrane tension or locally concentrating proteins such as endophilin.

We reiterate in passing that our shape stability theory describes the capacity of a peripheral protein to generate curvature not only with the well-known spontaneous curvature, but with two additional parameters related to molecular details of the protein / membrane system: the protein density for tubulating a tensionless membrane, and the maximal tubulation tension. In future contributions we will demonstrate that these parameters can vary significantly, comparing different types of proteins.

Shape stability boundary is unaffected by binding kinetics

We note that the biophysical shape stability fitted to our experimental data is valid only under thermodynamic equilibrium conditions – an assumption that needs verification. We therefore investigated if binding kinetics of proteins to the membrane measurably affects the transition-density.

Negatively charged PS lipids can affect the binding kinetics of proteins both *in vivo* and *in vitro*[18,33]. Specifically, a larger fraction of PS lipids in the membrane is known to increase the membrane binding rate of the endophilin N-BAR domain[18]. In order to test the thermodynamic equilibrium hypothesis, we measured the membrane shape transition points for vesicles containing different amounts of negatively charged lipids.

Not surprisingly, the equilibrium density of proteins on the membrane significantly increases with an increasing amount of PS lipids in GUVs (Fig. 5). Interestingly however, transition-densities, as well as the tension dependence, are identical within uncertainties for the three lipid compositions tested (Fig. 5 and Supplementary Figure 7). Equivalently, for the same lipid composition, only equilibrium densities, but not transition-densities, depend on bulk protein concentration (Supplementary Figure 5a). To further validate the hypothesis that membrane binding kinetics do not affect our results, we measured an apparent protein binding rate by determining the slope of the protein binding curve in a time interval close to the shape instability (Supplementary Figure 8a). Using GUVs under the same membrane tension (0.110 ± 0.007 mN·m^{-1}, Mean±SD), we found that transition-densities exhibit no dependence on the apparent protein binding rate (see Supplementary Figure 8b, showing a zero slope within statistical error (7.5±10s)). We therefore conclude that under our

conditions, protein-membrane binding kinetics plays a negligible role in controlling the membrane curvature instability.

Lipid shape as an additional control parameter

We finally asked if lipid shape can affect the shape transition-density for endophilin N-BAR. Figure 6 shows that the cone-shaped lipids cholesterol and DOPE both significantly reduce the transition-density at constant membrane tension. This amplification effect of cone-shaped lipids on membrane tubulation is consistent with previous observations in a different experimental system[26]. However, only the presence of DOPE but not cholesterol lowers the bending rigidity of the membrane (Supplementary Figure 6). Therefore, at least for cholesterol, we can attribute its effect on the transition-density to the conical lipid shape[34,35]. It is well known that proteins with membrane curvature insertion ability will lead to different spontaneous curvature of the membrane depending on the protein's insertion depth[36]. Therefore, in the presence of conical lipids, the protein's coupling strength to membrane curvature may be altered by allowing the protein to insert more deeply into the lipid bilayer – a hypothesis that remains to be tested. In addition to membrane tension and protein density, lipid shape provides a third level of control that cells can use to regulate membrane shape transitions (Fig. 7).

Discussion

It has to be emphasized that we have used the simplest thermodynamic theory of membrane stability in the presence of curvature-inducing proteins, which neglects the highly anisotropic spontaneous curvature and significant oligomerization tendency of N-BAR domain proteins[18,37–40]. Nevertheless, our model accurately describes the shape transition. Precisely because the model does not assume details about the protein other than the curvature-coupling strength and an excluded area for the protein, it likely applies to all endocytic proteins.

The presence of a well-defined membrane shape transition-density provides an attractive explanation for how endocytic protein recruitment can control plasma membrane deformation during CME: the initiation of membrane buds and the formation of a CCV may proceed only after establishing well defined transition-densities of endocytic proteins. For UFE, however, the endocytic vesicle formation route of a 10 millisecond duration leaves little time for a plasma membrane patch to undergo a sequential protein recruitment process as in CME (typically 10~20s[2]). Thus, instead of recruiting additional curvature generating proteins to the membrane, for the case of UFE, a more plausible signal that triggers membrane budding is the lowering of membrane tension in the presence of already membrane-bound peripheral proteins. Due to the membrane fluidity, tension changes propagate at a speed of about $10^6 \mu m \cdot s^{-1}$ [11,41]. Therefore, a tension reduction caused by processes such as the fusion of exocytic vesicles into the plasma membrane can likely trigger endocytosis at a much faster rate compared to the process of recruiting peripheral curvature-inducing proteins. For classical endocytosis, a checkpoint that separates abortive from propagating endocytic pits has been identified[42,43]. It is possible that the stability boundary identified in our shape diagram provides a mechanistic explanation for this

phenomenon. Abortive endocytic pits might assemble due to local fluctuations in protein density and membrane tension, but in situations where the stability boundary is not passed such fluctuations will eventually decay without producing vesicles.

Our findings provide new insights into how cellular membrane shapes and dynamics are controlled by interacting with curvature-coupling proteins as well as via the regulation of membrane physical properties such as tension and lipid shape. We suggest that the coupling of membrane tension and density of curvature-coupling proteins determined here plays modulatory roles in all forms of endocytosis.

Methods

Materials

Lipids 1,2-dioleoyl-sn-glycero-3-phosphocholine (DOPC), 1,2-dioleoyl-*sn*-glycero-3-phospho-L-serine (DOPS), 1,2-dioleoyl-*sn*-glycero-3-phosphoethanolamine (DOPE), Cholesterol (Chol), and Distearoylphosphatidylethanolamine-N-(biotinyl(polyethylene glycol)2000) (DSPE-Bio-574 PEG2000) were obtained from Avanti Polar Lipids (Alabaster,AL). Alexa Fluor® 488 (AF-488) C5-maleimide, BODIPY® FL DHPE (N-(4,4-Difluoro-5,7-Dimethyl-4-Bora-3a,4a-Diaza-s-Indacene-3-Propionyl)-1,2-Dihexadecanoyl-sn-Glycero-3-Phosphoethanolamine, Triethylammonium Salt) and Texas Red-1,2-dihexadecanoyl-sn-glycero-3 phosphoethanolamine (triethylammonium salt) were from Invitrogen/Life Technologies (Grand Island, NY). Casein, Tris, HEPES, and EDTA were obtained from Fisher Scientific (Rochester, NY). All commercial reagents were used without further purification. Streptavidin conjugated microspheres with mean diameter of ~6μm were from Polysciences, Inc. (Warrington, PA). An additional 0.5% DSPE-Bio-574 PEG2000 was added into the lipid mixture when preparing GUVs for membrane bending rigidity measurements through tether pulling. Rat endophilin A1 N-BAR_C241 (residues 1–247) and full-length endophilin A1 were expressed, purified and labelled with AF-488 as described[18,23]. Protein concentrations were determined by Bradford analysis using bovine serum albumin (Thermo) as a standard. Concentrations indicated refer to total concentration of endophilin in terms of dimeric units.

Imaging chamber preparation and GUV transfer procedures

GUVs were prepared in 300mM sucrose solution by the standard method of electroformation with 0.3%Texas Red-DHPE in desired lipid compositions, using indium tin oxide covered glass slides onto which thin films of lipids were prepared from chloroform solutions[44]. Two imaging chambers, GUV chamber and protein chamber, were formed between two coverslips (20mm×40mm, pre-treated with 2μL of 2.5mg·ml^{-1} casein, 20mM Tris, and 2mM EDTA) overhanging a glass microscope slide (2mm thick). The GUV chamber has a total volume of 375μL and is made by diluting 5~8μL of the GUV stock solutions into a buffer containing glucose, sucrose, NaCl and HEPES. The osmolarity of the buffer was selected to be 20% higher than the GUV stock solution (measured with a micro-osmometer Advanced Instruments Inc. (Norwood, MA)) to ensure that the vesicles had enough excess area for micropipette aspiration. The protein chamber had a total volume of 187.5μL. The protein stock solution was diluted to designated concentrations, using the

same buffer as used for diluting GUVs. For both chambers, we chose pH = 7 and NaCl was kept at 50mM, with 7mM HEPES. Sucrose and glucose (1:1) concentrations were adjusted to yield total osmolarities of the desired values. Micropipettes and transfer capillaries were prepared and casein-treated through incubation with saturated casein solutions followed by rinsing[18,44]. Occasionally, GUV membranes were observed to stick to pipette walls. Data from such vesicles were discarded.

The GUV transfer was a four-step process as shown in Figure 1b: ① A GUV was aspirated into a micropipette to adjust the desired membrane tension. ② The transfer capillary was manually positioned to cover the GUV. ③ The GUV was transferred from the GUV chamber into the protein chamber using a motor-controlled micromanipulator (Luigs and Neumann, Ratingen, Germany). ④ The transfer capillary was removed to expose the GUV to protein. The moment when the GUV was not protected anymore by the transfer capillary was defined as time zero in the protein-GUV association analysis. Zero aspiration pressure was checked before and after the protein-GUV association process to ensure absence of pressure drifts[45]. All the transfer and imaging processes were carried out at room temperature (23.7±0.3 °; Mean±SD measured on different days).

Microscopy and data analysis

The protein-membrane association process and the membrane geometry changes were monitored with a confocal fluorescence microscope[44], using a 60× 1.1 N.A. objective (Olympus, Center Valley, PA). The aspiration length, L_p, micropipette radius, R_p and GUV radius, R_v were measured with Image J, as illustrated in Figure 1a. The GUV geometry was calculated as $\text{Area}(t) = 4\pi R_v(t)^2 + 2\pi R_p L_p(t)$, $\text{Volume}(t) = 4\pi R_v(t)^3/3 + \pi R_p^2 L_p(t)$. The average protein fluorescence intensity was determined by fitting a Gaussian ring to the GUV contour (excluding the aspirated region) using MATLAB. R_v can also be obtained from the fitting and was checked with the direct measurement in Image J.

The measured fluorescence intensity was then converted to protein number density ρ(t) on the membrane, using the method of Ref.[19], as follows. GUVs containing *x*% BODIPY and (100-*x*)% DOPC were prepared (*x*: 0.1~0.7) and at least ten independent GUVs were imaged under the same settings as during the recording of GUV-protein association. A linear fit (r^2=0.99) was carried out to get the relation between measured GUV fluorescence intensity and BODIPY density on the membrane. The quantum yield difference between BODIPY and AF-488 was determined to be BODIPY/'AF-488'=0.5, by imaging bulk solution intensity of SUVs (containing BODIPY) and AF-488 labelled proteins under the same solution conditions as in our experiments (50mM NaCl, pH 7)[46]. The average lipid headgroup area was assumed as 0.7 nm^2. The relation between imaged average fluorescence intensity (FL, in arbitrary units for 16-bit images) and dimeric endophilin N-BAR density (ρ in the unit of μm^{-2} and with a labelling efficiency LE) on GUVs is: FL/LE =(4.9±0.2)×ρ.

The membrane shape transition point t_c was defined as the time point when *Area(t)* begins to decrease (Fig. 2), and the corresponding protein density $\rho(t_c)$ was defined as the transition-density.

Membrane bending rigidity measurements

A 1mm thick sample chamber was formed by overhanging two coverslips on both sides of a microscope glass slide. The bottom of the chamber was pre-treated with 2μL of 2.5mg·ml^{-1} casein in 20mM Tris-HCl and 2mM EDTA to prevent adhesion of beads and GUVs to the coverslip. The chamber was filled with 1μL of microsphere dispersion, 5μL of GUV dispersion, and 90~100μL of the same sucrose, glucose, NaCl and HEPES mixture as described above, resulting a final environment containing 50mM NaCl. The chamber was mounted on an inverted microscope (1×71; Olympus, Center Valley, PA) equipped with a home built optical trap as described in refs[45,46]. A GUV (about 10μm in radius) was aspirated at a constant pressure and subsequently brought into contact with a trapped bead. Then the bead was moved at 10μm·s^{-1} to pull out a membrane tether of 20μm in length. The tether pulling force f is determined as for a Hookean spring: $f = k\Delta x$, where k is the trap stiffness and Δx is the displacement of the bead relative to its equilibrium position. The stiffness of the trap with a typical value of 0.05pN·nm^{-1} was calibrated by the drag-force method[47] for multiple beads. Aspiration pressure was changed after the formation of a stable tether to obtain the relation between tether pulling force and membrane lateral tension. Each lateral tension was maintained until the pulling forces reached equilibrium (typically a few seconds). Membrane bending rigidity was subsequently extracted from the relation: $f=2\pi\sqrt{2\kappa\sigma}$ [48]. For each lipid composition used, force-tension relations and thus bending rigidities were measured on tethers pulled from at least five independent GUVs.

Supplementary Material

Refer to Web version on PubMed Central for supplementary material.

Acknowledgments

We are grateful for funding from NIH grant GM 097552 and NSF grant CBET 1053857. Furthermore we thank Z. Chen and B. Capraro for the help with protein preparations and thank T. Wu and N. Li for comments on a manuscript draft.

References

1. Bonifacino JS, Glick BS. The mechanisms of vesicle budding and fusion. Cell. 2004; 116:153–166. [PubMed: 14744428]
2. Taylor MJ, Perrais D, Merrifield CJ. A High Precision Survey of the Molecular Dynamics of Mammalian Clathrin-Mediated Endocytosis. Plos Biology. 2011; 9 doi:e100060410.1371/journal.pbio.1000604.
3. McMahon HT, Boucrot E. Molecular mechanism and physiological functions of clathrin-mediated endocytosis. Nature Reviews Molecular Cell Biology. 2011; 12:517–533. [PubMed: 21779028]
4. Kononenko, Natalia L., et al. Clathrin/AP-2 Mediate Synaptic Vesicle Reformation from Endosome-like Vacuoles but Are Not Essential for Membrane Retrieval at Central Synapses. Neuron. 2014; 82:981–988. [PubMed: 24908483]
5. Morris CE, Homann U. Cell Surface Area Regulation and Membrane Tension. The Journal of Membrane Biology. 2001; 179:79–102. [PubMed: 11220366]
6. Schweitzer Y, Lieber Arnon D, Keren K, Kozlov Michael M. Theoretical Analysis of Membrane Tension in Moving Cells. Biophys J. 2014; 106:84–92. [PubMed: 24411240]

7. Pietuch A, Bruckner BR, Fine T, Mey I, Janshoff A. Elastic properties of cells in the context of confluent cell monolayers: impact of tension and surface area regulation. Soft Matter. 2013; 9:11490–11502.
8. Raucher D, Sheetz MP. Membrane expansion increases endocytosis rate during mitosis. Journal of Cell Biology. 1999; 144:497–506. [PubMed: 9971744]
9. Masters TA, Pontes B, Viasnoff V, Li Y, Gauthier NC. Plasma membrane tension orchestrates membrane trafficking, cytoskeletal remodeling, and biochemical signaling during phagocytosis. Proceedings of the National Academy of Sciences of the United States of America. 2013; 110:11875–11880. [PubMed: 23821745]
10. Diz-Munoz A, Fletcher DA, Weiner OD. Use the force: membrane tension as an organizer of cell shape and motility. Trends in Cell Biology. 2013; 23:47–53. [PubMed: 23122885]
11. Keren K, et al. Mechanism of shape determination in motile cells. Nature. 2008; 453 475-U471.
12. Gauthier NC, Fardin MA, Roca-Cusachs P, Sheetz MP. Temporary increase in plasma membrane tension coordinates the activation of exocytosis and contraction during cell spreading. Proceedings of the National Academy of Sciences of the United States of America. 2011; 108:14467–14472. [PubMed: 21808040]
13. Watanabe S, et al. Ultrafast endocytosis at mouse hippocampal synapses. Nature. 2013; 504:242–247. [PubMed: 24305055]
14. Thiam AR, et al. COPI buds 60-nm lipid droplets from reconstituted water-phospholipid-triacylglyceride interfaces, suggesting a tension clamp function. Proceedings of the National Academy of Sciences of the United States of America. 2013; 110:13244–13249. [PubMed: 23901109]
15. Boulant S, Kural C, Zeeh JC, Ubelmann F, Kirchhausen T. Actin dynamics counteract membrane tension during clathrin-mediated endocytosis. Nature Cell Biology. 2011; 13 1124-U1158, doi:Doi 10.1038/Ncb2307.
16. Houk, Andrew R., et al. Membrane Tension Maintains Cell Polarity by Confining Signals to the Leading Edge during Neutrophil Migration. Cell. 2012; 148:175–188. [PubMed: 22265410]
17. Manneville JB, et al. COPI coat assembly occurs on liquid-disordered domains and the associated membrane deformations are limited by membrane tension. Proceedings of the National Academy of Sciences of the United States of America. 2008; 105:16946–16951. doi:DOI 10.1073/pnas.0807102105. [PubMed: 18974217]
18. Capraro BR, et al. Kinetics of endophilin N-BAR domain dimerization and membrane interactions. Journal of Biological Chemistry. 2013
19. Sorre B, et al. Nature of curvature coupling of amphiphysin with membranes depends on its bound density. Proceedings of the National Academy of Sciences of the United States of America. 2012; 109:173–178. [PubMed: 22184226]
20. Mim C, et al. Structural Basis of Membrane Bending by the N-BAR Protein Endophilin. Cell. 2012; 149:137–145. doi:DOI 10.1016/j.cell.2012.01.048. [PubMed: 22464326]
21. Baumgart, T.; Capraro, BR.; Zhu, C.; Das, SL. Annual Review of Physical Chemistry, Vol 62 Vol. 62. In: Leone, SR.; Cremer, PS.; Groves, JT.; Johnson, MA., editors. Annual Review of Physical Chemistry. 2011. p. 483-506.
22. van Meer G, Voelker DR, Feigenson GW. Membrane lipids: where they are and how they behave. Nature Reviews Molecular Cell Biology. 2008; 9:112–124. [PubMed: 18216768]
23. Chen Z, et al. Intradimer/Intermolecular Interactions Suggest Autoinhibition Mechanism in Endophilin A1. Journal of the American Chemical Society. 2014; 136:4557–4564. [PubMed: 24568626]
24. Sens P, Turner MS. Budded membrane microdomains as tension regulators. Physical Review E. 2006; 73 doi:03191810.1103/PhysRevE.73.031918.
25. Lipowsky R. Spontaneous tubulation of membranes and vesicles reveals membrane tension generated by spontaneous curvature. Faraday Discussions. 2013; 161:305–331. [PubMed: 23805747]
26. Stachowiak JC, Hayden CC, Sasaki DY. Steric confinement of proteins on lipid membranes can drive curvature and tubulation. Proceedings of the National Academy of Sciences of the United States of America. 2010; 107:7781–7786. [PubMed: 20385839]

27. Shi Z, Baumgart T. Dynamics and instabilities of lipid bilayer membrane shapes. Advances in Colloid and Interface Science. 2014
28. Seifert U. Configurations of fluid membranes and vesicles. Advances in Physics. 1997; 46:13–137.
29. Bhatia VK, et al. Amphipathic motifs in BAR domains are essential for membrane curvature sensing. Embo Journal. 2009; 28:3303–3314. [PubMed: 19816406]
30. Cahn JW, Hilliard JE. FREE ENERGY OF A NONUNIFORM SYSTEM .1. INTERFACIAL FREE ENERGY. Journal of Chemical Physics. 1958; 28:258–267.
31. Zhu C, Das SL, Baumgart T. Nonlinear Sorting, Curvature Generation, and Crowding of Endophilin N-BAR on Tubular Membranes. Biophysical Journal. 2012; 102:1837–1845. doi:DOI 10.1016/j.bpj.2012.03.039. [PubMed: 22768939]
32. Wilhelm BG, et al. Composition of isolated synaptic boutons reveals the amounts of vesicle trafficking proteins. Science. 2014; 344:1023–1028. [PubMed: 24876496]
33. Bohdanowicz M, Grinstein S. ROLE OF PHOSPHOLIPIDS IN ENDOCYTOSIS, PHAGOCYTOSIS, AND MACROPINOCYTOSIS. Physiological Reviews. 2013; 93:69–106. [PubMed: 23303906]
34. Zimmerberg J, Kozlov MM. How proteins produce cellular membrane curvature. Nature Reviews Molecular Cell Biology. 2006; 7:9–19. [PubMed: 16365634]
35. Chen Z, Rand RP. The influence of cholesterol on phospholipid membrane curvature and bending elasticity. Biophys J. 1997; 73:267–276. [PubMed: 9199791]
36. Campelo F, McMahon HT, Kozlov MM. The hydrophobic insertion mechanism of membrane curvature generation by proteins. Biophys J. 2008; 95:2325–2339. [PubMed: 18515373]
37. Kabaso D, et al. On the role of membrane anisotropy and BAR proteins in the stability of tubular membrane structures. Journal of Biomechanics. 2012; 45:231–238. [PubMed: 22138195]
38. Walani N, Torres J, Agrawal A. Anisotropic spontaneous curvatures in lipid membranes. Physical Review E. 2014; 89 doi:06271510.1103/PhysRevE.89.062715.
39. Cui H, et al. Understanding the Role of Amphipathic Helices in N-BAR Domain Driven Membrane Remodeling. Biophysical Journal. 2012; 104:404–411. [PubMed: 23442862]
40. Hiroshi N. Two- or three-step assembly of banana-shaped proteins coupled with shape transformation of lipid membranes. EPL (Europhysics Letters). 2014; 108:48001.
41. Dommersnes PG, Orwar O, Brochard-Wyart F, Joanny JF. Marangoni transport in lipid nanotubes. Europhysics Letters. 2005; 70:271–277.
42. Ehrlich M, et al. Endocytosis by random initiation and stabilization of clathrin-coated pits. Cell. 2004; 118:591–605. [PubMed: 15339664]
43. Loerke D, et al. Cargo and Dynamin Regulate Clathrin-Coated Pit Maturation. Plos Biology. 2009; 7:628–639. doi:e100005710.1371/journal.pbio.1000057.
44. Tian A, Baumgart T. Sorting of lipids and proteins in membrane curvature gradients. Biophysical Journal. 2009; 96:2676–2688. [PubMed: 19348750]
45. Heinrich M, Tian A, Esposito C, Baumgart T. Dynamic sorting of lipids and proteins in membrane tubes with a moving phase boundary. Proceedings of the National Academy of Sciences of the United States of America. 2010; 107:7208–7213. [PubMed: 20368457]
46. Wu T, Shi Z, Baumgart T. Mutations in BIN1 Associated with Centronuclear Myopathy Disrupt Membrane Remodeling by Affecting Protein Density and Oligomerization. PLoS ONE. 2014; 9:e93060. [PubMed: 24755653]
47. Svoboda K, Block SM. Biological Applications of Optical Forces. Annu Rev Bioph Biom. 1994; 23:247–285.
48. Derenyi I, Julicher F, Prost J. Formation and interaction of membrane tubes (vol 88, art no 238101, 2002). Physical Review Letters. 2002; 89 doi:20990110.1103/PhysRevLett.89.209901.

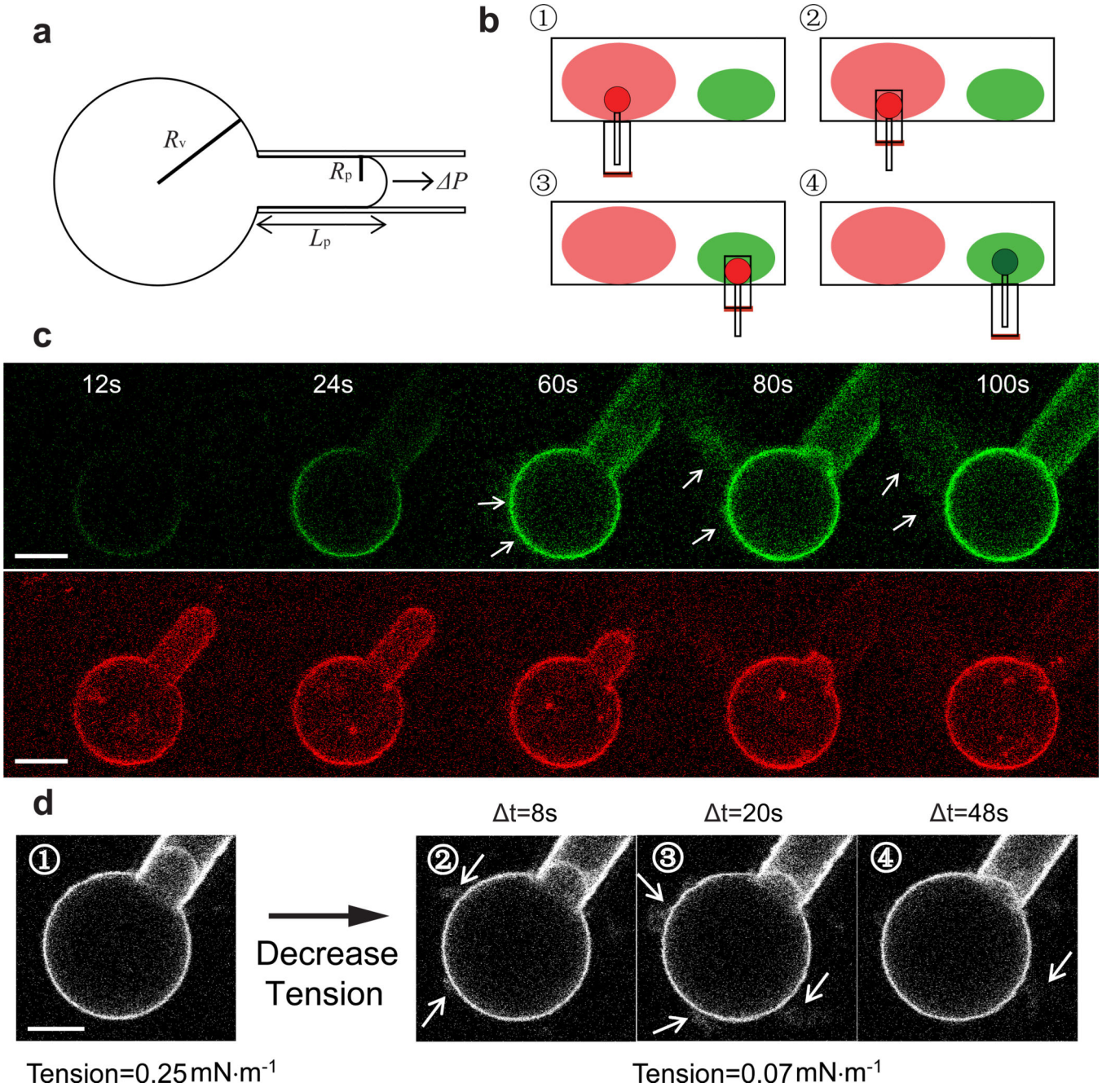

Figure 1. Endophilin N-BAR domain induced membrane tubulation of GUV

(a) Sketch of a micro-pipette aspirated GUV. ΔP is the pressure difference between inside and outside of the pipette used for GUV aspiration. R_p and R_v represent the pipette radius and the radius of the spherical part of the GUV, respectively, L_p represents the aspiration length of the GUV. (b) The process of transferring an aspirated GUV from the GUV dispersion (red) into a protein solution (green) (also see Methods). (c) Time lapse confocal images showing the formation of tubes (after t=24s, as indicated by arrows) and the change in aspiration length during endophilin N-BAR binding. Membrane tension was held constant at 0.05 $mN \cdot m^{-1}$. Green: protein channel; Red: lipid channel. (d) ① A GUV incubated to

equilibrium with endophilin N-BAR under high tension (0.25 $mN \cdot m^{-1}$). After equilibration, tension was reduced to 0.07 $mN \cdot m^{-1}$ within 2 seconds. Membrane tubes as indicated by arrows can be observed on the GUV under low membrane tension (0.07 $mN \cdot m^{-1}$) for Δt equal to ② 8s; ③ 20s; ④ 48s ($\Delta t=0$ is defined as the time point of tension reduction). Scale bars: 10 μm.

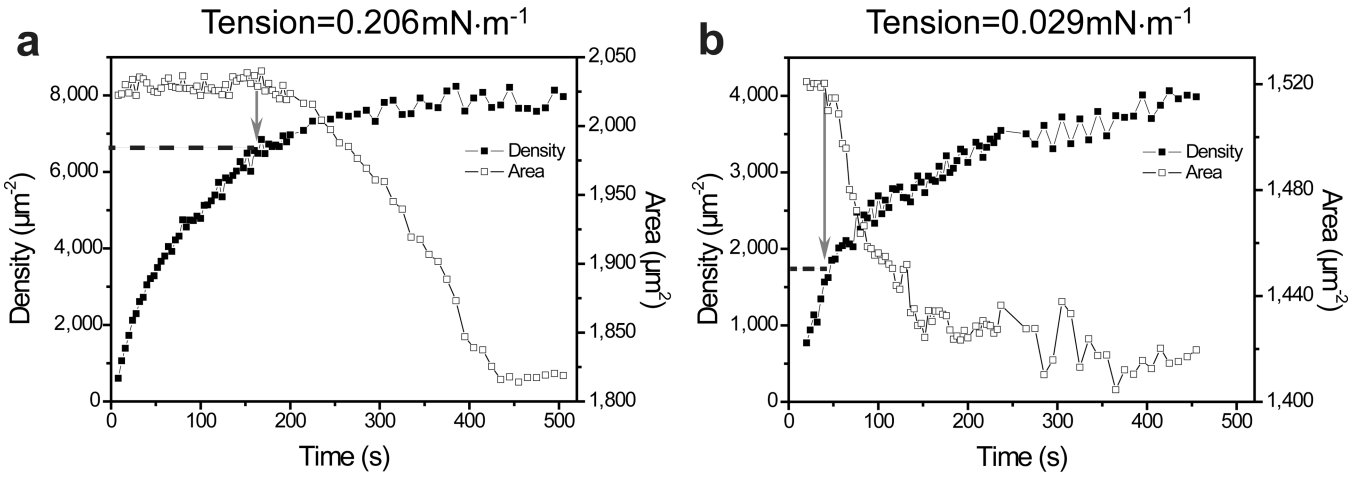

Figure 2. Membrane tension and bound protein density modulate membrane shape transition

(a) A representative trial with high (0.206 $mN \cdot m^{-1}$) membrane tension, the membrane-bound endophilin N-BAR density at the onset of area decrease (as indicated by the arrow) genuinely reveals the shape transition point. The area is calculated from the time-dependent aspiration length and vesicle radius as shown in Supplementary Figure 2b. (b) A representative trial with low (0.029 $mN \cdot m^{-1}$) membrane tension. Transition-density (marked by the dashed lines) decreased significantly compared to the high tension case shown in (a). Bulk concentrations of endophilin N-BAR are 150nM in (a) and 75nM in (b). Potential influence of bulk protein concentration on transition-densities was eliminated by comparing the transition-densities of similar tension GUVs in endophilin N-BAR solutions of various bulk concentrations (Supplementary Figure 5a). Additionally, there was no observable influence of membrane tension on the endophilin N-BAR's equilibrium density on GUVs (Supplementary Figure 5b).

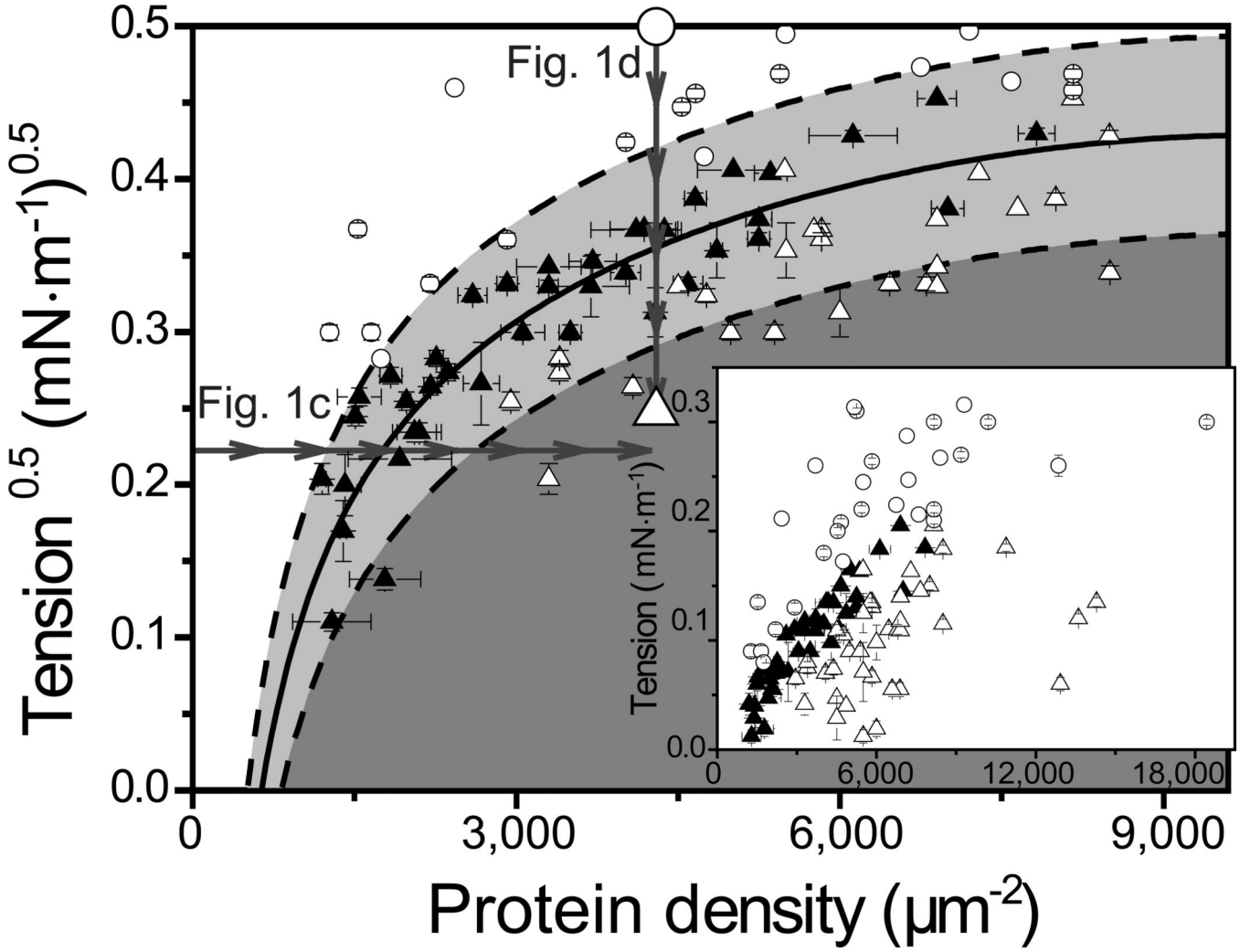

Figure 3. Experimental shape stability diagram agrees well with curvature instability theory

Filled triangles represent the measured transition-density (expressed as a cover fraction, using the close-packed N-BAR dimer density of 30000 μm^{-2})[29] of GUVs under corresponding tensions. The open data points represent the maximum protein cover fraction reached by a GUV with (triangle) or without (circle) tubulation during protein-membrane binding. The solid line represents the best fit of experimental data with the proposed curvature instability model (r^2=0.85). The dashed lines are 95% confidence intervals for the fit. The shaded area represents the region where the membrane is tubulated by endophilin N-BAR. The arrows indicate two ways of inducing membrane tubulation: 1), by increasing protein coverage on the membrane at constant tension or 2), by decreasing membrane tension at constant coverage. The large circle (non-tubulated state), and triangle (tubulated state), represent the state of the membrane before and after tension reduction (compare Figure 1d), respectively. The inset shows the same data using linear axes. Error bars represent the standard errors associated with determining each data point. Concentrations of endophilin N-BAR used in the experiment ranged from 25nM to 400nM (also note Supplementary Figure 5a).

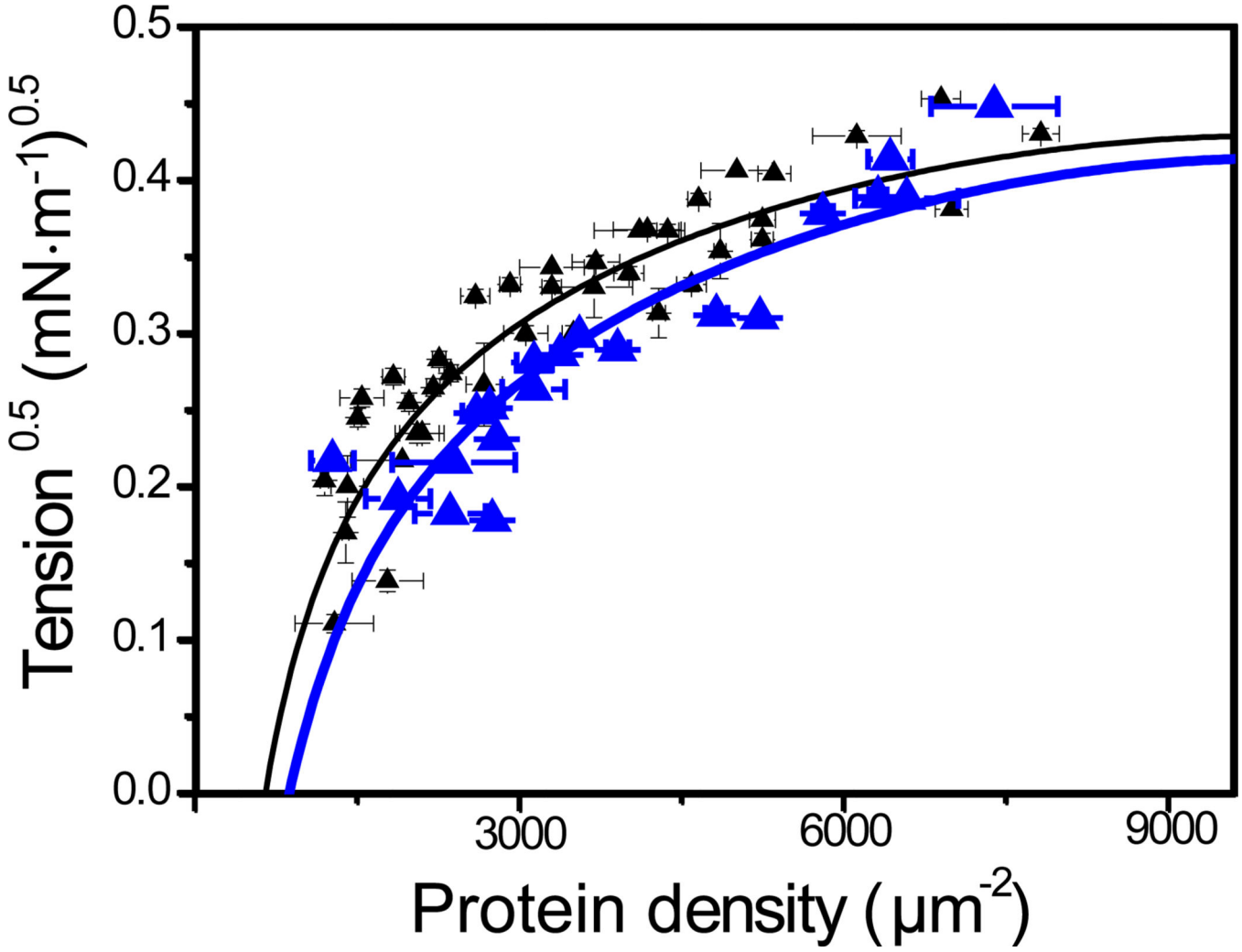

Figure 4. Full length protein shows smaller curvature generation capacity than N-BAR

Transition-densities of full length endophilin (blue triangles) as well as the best fit with our curvature instability model (blue line, r^2=0.75) are plotted on top of the stability diagram of N-BAR displayed in Figure 3 for GUVs with the same lipid composition (DOPS/DOPE/DOPC = 45/30/25). The physical properties resulting from fitting the endophilin full length data are: the spontaneous curvature C_0^{-1} = 6.1±1.1nm; the upper tension limit σ* = 0.17±0.04 mN·m^{-1}; the protein transition-density required for tubulating a tensionless membrane ρ_0 = 850±300μm^{-2}. P=0.035 between the stability boundaries of endophilin full length and N-BAR via f-test. Error bars represent the standard errors associated with determining each data point.

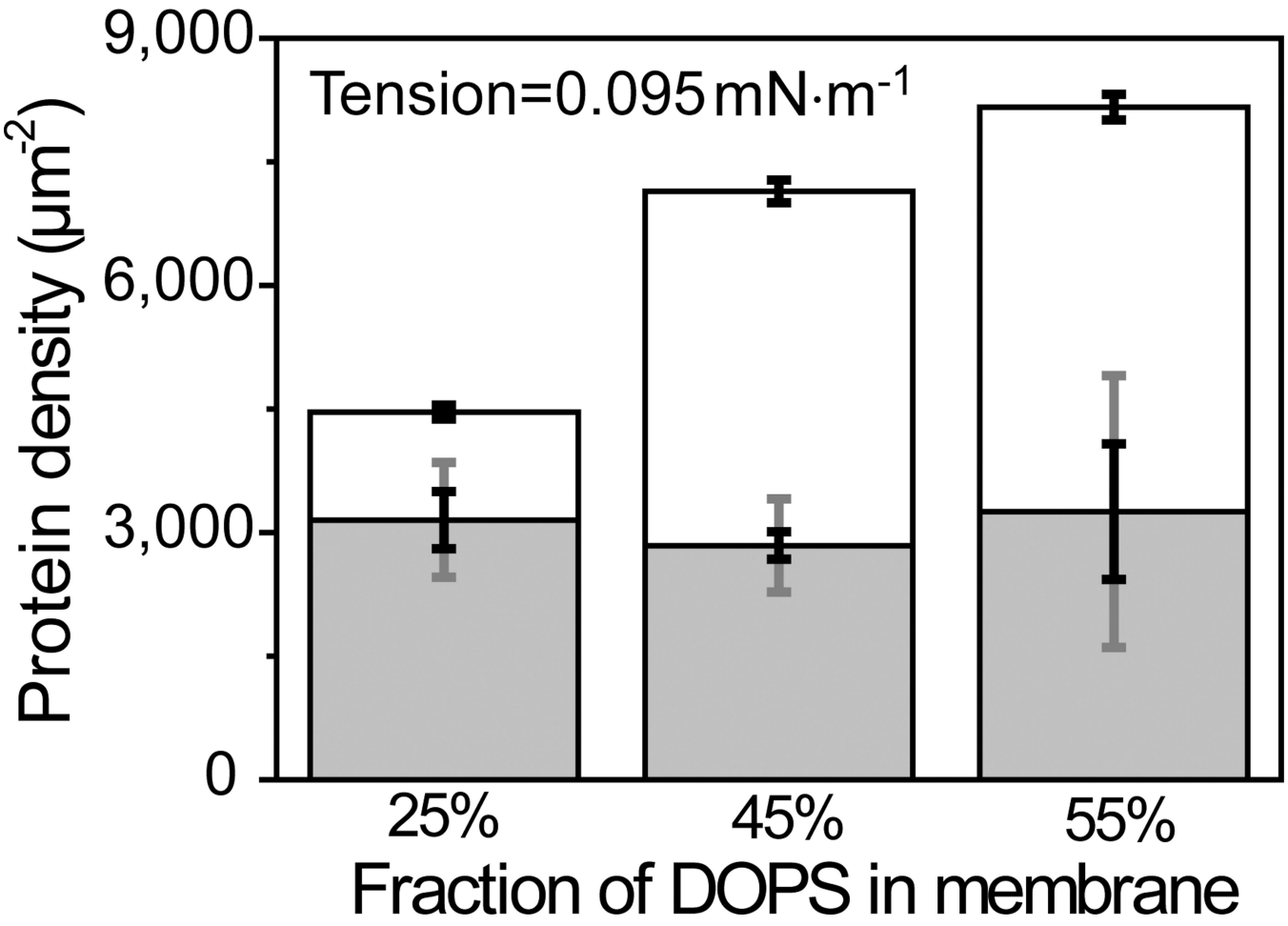

Figure 5. Membrane charge affects equilibrium density, not transition density

Equilibrium densities of endophilin N-BAR (open bars) increase significantly for increasing amounts of DOPS in the GUV (for each composition pair $P<10^{-4}$, Student t test). No significant difference can be found among the transition densities (gray bars, for each composition pair, $P>0.5$, Student t test). Concentration of endophilin N-BAR domain: 100nM. GUV compositions: DOPS/DOPE/DOPC = X/30/(70-X). All GUVs considered here are at the membrane tension of 0.095 ± 0.013 mN·m^{-1} (Mean ± SD). Gray error bars are standard deviations (SD) of the data and black error bars are standard errors of the mean (SEM), same below.

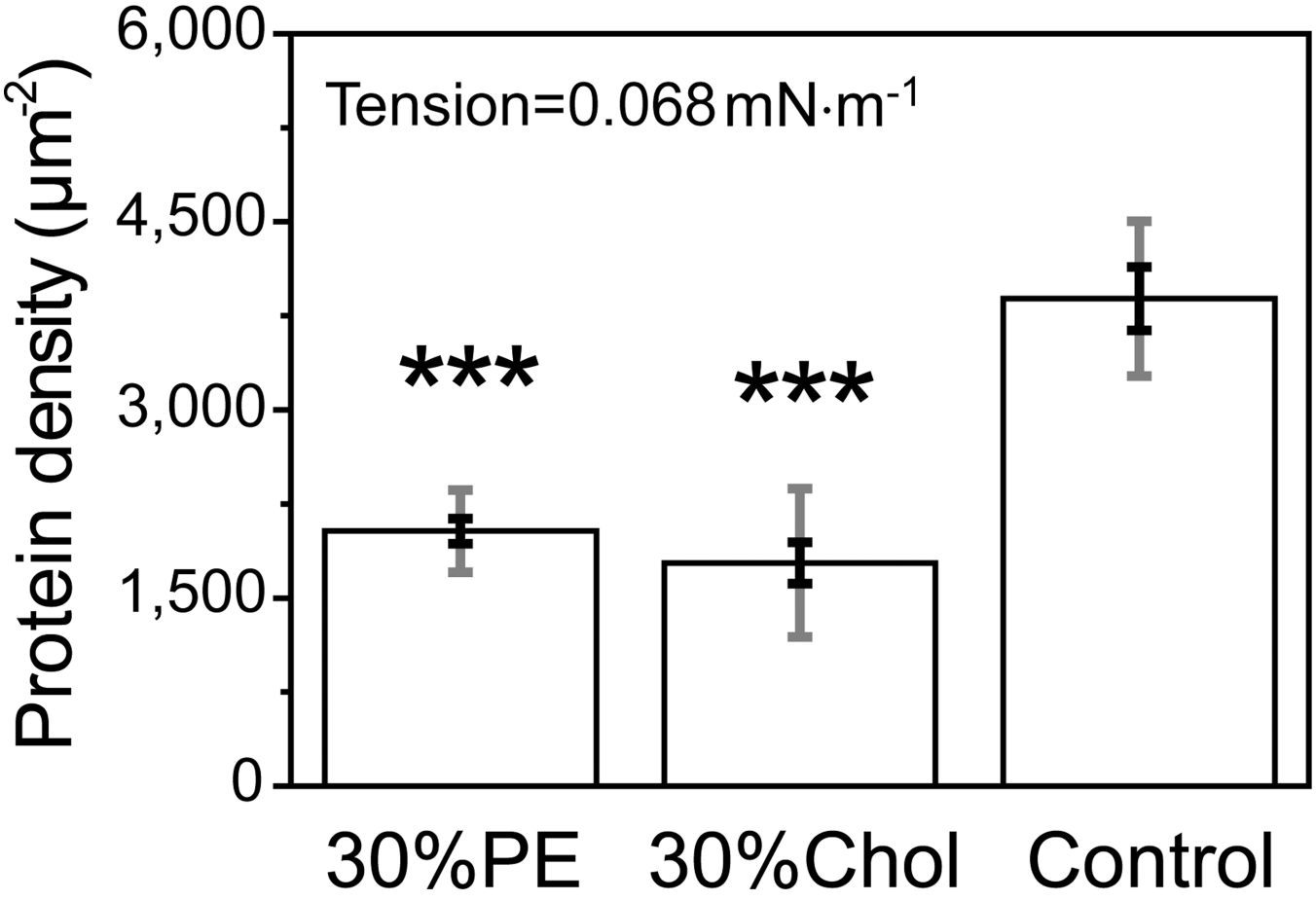

Figure 6. The effect of conical lipids on membrane shape transitions

Under the same membrane tension (0.068 ± 0.007 $mN \cdot m^{-1}$ (Mean ± SD))), the presence of 30% conical lipids, either DOPE or cholesterol, significantly lowers the transition-density of endophilin N-BAR domain. ***$P<10^{-4}$, Student t test.

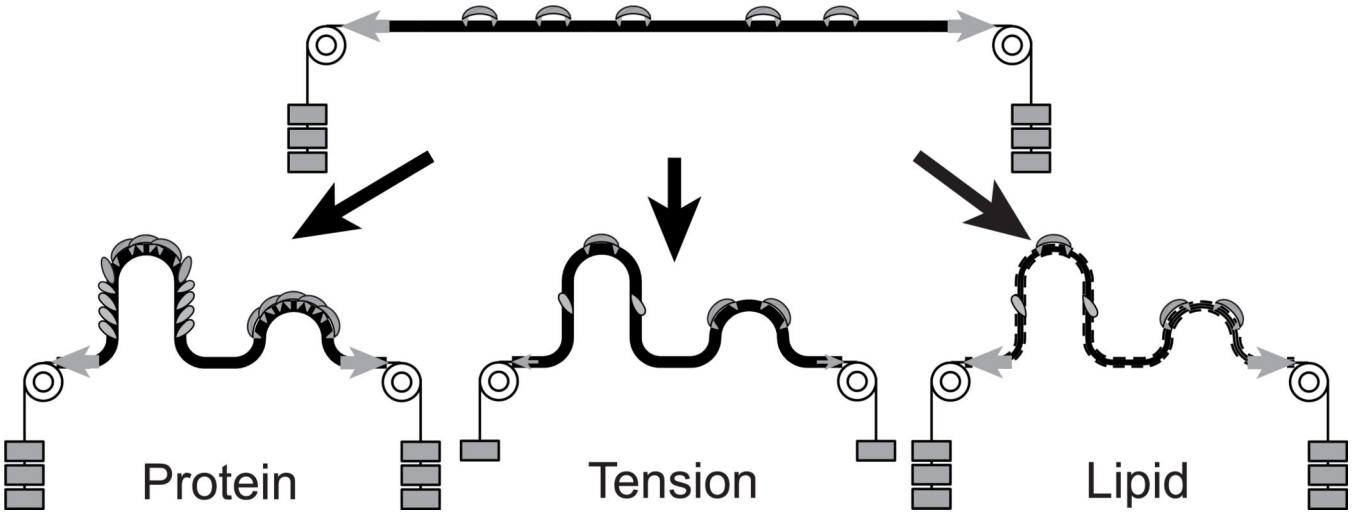

Figure 7. Three ways of mediating membrane curvature instability

Three regulatory elements are identified in this contribution that can modulate membrane shape transitions induced by the binding of curvature coupling proteins. Notably, membrane budding and tubulation is not solely induced by protein association (left arrow). The effects of lowering membrane tension (middle arrow) and changing membrane lipid composition (right arrow) also control membrane shape transition without the assistance of additional proteins. The contribution of peripheral proteins is defined by their density on the membrane, emphasizing a thermodynamic role played by protein molecules in mediating membrane shape transitions. The tension effect may explain an ultrafast pathway cells can utilize to control membrane shape transformations such as endocytosis.